Turkish Journal of Electrical Engineering & Computer Sciences

http://journals.tubitak.gov.tr/elektrik/

Research Article

Turk J Elec Eng & Comp Sci
(2018) 26: 2178 – 2193

doi:10.3906/elk-1802-52

Region characteristics-based fusion of spatial and transform domain image denoising methods

Rajiv VERMA*, **Rajoo PANDEY**
Department of Electronics and Communication Engineering, National Institute of Technology Kurukshetra, Kurukshetra, India

Received: 18.02.2018 • **Accepted/Published Online:** 26.05.2018 • **Final Version:** 28.09.2018

Abstract: Nonlocal means (NLM)- and wavelet-based image denoising methods have drawn much attention in image processing due to their effectiveness and simplicity. The performance of these algorithms varies according to region characteristics in an image. For example, NLM performs well for smooth regions due to deployment of redundancy available in images, whereas wavelet-based approaches may preserve key image features by controlling the degree of threshold for shrinking the noisy coefficients. This paper presents a simple novel approach that estimates an original image by simply taking the weighted average of the denoised images pixel values obtained by NLM and wavelet thresholding schemes based on natural characteristics of regions in an image. Extensive simulations on standard images demonstrate that the proposed approach outperforms the benchmark wavelet-based schemes, NLM and its variants, in terms of peak signal-to-noise ratio (PSNR(dB)), mean structural similarity metric (MSSIM), and visual quality.

Key words: Image denoising, bilateral filter, nonlocal means, wavelet, region characteristics

1. Introduction

Noise is generally produced in digital images/videos during acquisition and transmission process due to imperfections in imaging devices and other environmental conditions, respectively. No matter how good digital imaging devices are, improvement in image quality is always needed in practice [1, 2]. Therefore, manufacturers of imaging devices rely on developing efficient and less complex image denoising algorithms to restore the degraded images. Due to intrinsic connection between denoising and other tasks such as segmentation, recognition, and tracking, image denoising is still an active and fundamental research problem in the field of image processing [3].

In the last two decades, several linear and nonlinear filters in spatial and transform domain have been proposed to resolve the denoising problem effectively [4, 5]. Among them, bilateral filter [6, 7], nonlocal means (NLM) [8, 9], and wavelet shrinkage methods [10, 11] are widely used due to exploitation of the redundancy and sparsity in an image, respectively. Tomasi et al. [6] proposed a bilateral filter (BF) in which the weights are computed based on spatial distance and range or photometric distance to suppress the noise from images. The denoising performance of BF is very sensitive to photometric distance rather than spatial distance, which is generally computed directly from the noisy image. Recently, an entropy-based bilateral filter (EBF) is proposed, where a new range kernel is derived by exploiting the information from the filtered image and its corresponding method noise [7]. The NLM algorithm utilizes the similarity between the patches in the search region to assign

*Correspondence: rajiv_6120043@nitkkr.ac.in

weights to pixels in the averaging process [8]. The NLM algorithm is equivalent to bilateral filter, when the patch size reduces to pixel size. There are several critical issues regarding the NLM algorithm such as patch size, search region size, weight calculation, smoothing parameter, and computational complexity, which are still being researched [12]. Several variants of the NLM algorithm have been developed to handle these issues effectively [13–20]. Wavelet transform has become a popular and efficient tool for image denoising due to its various properties such as energy compaction, orthogonality, low complexity, and linearity [21]. The performance of wavelet-based approaches is affected by various parameters such as the choice of wavelets, threshold estimation, and shrinkage rules. A major part of the literature concerning wavelet-based approaches is devoted to handle the issue of threshold selection [11], which plays a crucial role in preservation of image details. Several popular benchmark shrinkage methods such as wiener filtering [22], VisuShrink [23, 24], SUREShrink [25], NeighShrink [26], BayesShrink [27], NeighSUREShrink [28], LAWML [29], BiShrink [30], IIDMWT [31], IAWDMNC [32], GIDMNWC [33], and LAPB [34] have been proposed to estimate the threshold for shrinking the noisy wavelet coefficients.

Generally, NLM-based methods and wavelet-based approaches utilize inter-patch and intra-patch correlations, respectively, for denoising the images. Another class of patch-based image denoising techniques such as Nonlocal Bayes (NL-Bayes) [35], block matching in three dimensions (BM3D) [36], and data adaptive dual domain denoising (DA3D) [37] have been developed, which exploit both intra-patch and inter-patch correlations to provide significantly improved denoising performance. However, the computational complexity of these algorithms is very high due to their iterative nature. At each iteration, the nonlocal self similarity in the filtered image is utilized to effectively estimate the sparse coefficients for better performance. As these algorithms require a large number of parameters for effective denoising, tunning these parameters is a challenging task for these algorithms. Furthermore, it is observed that these methods do not provide promising denoising results for texture images due to lack of redundancy in the regions containing image details [38]. Therefore, it is desirable to develop a denoising technique that can perform well for texture images and does not have very high complexity.

As the computational complexity of the NLM- and wavelet-based methods is much less than that of the patch-based denoising methods such as NL-Bayes, BM3D, and DA3D, this paper aimed at combining the best features of the NLM- and wavelet-based methods for effective image denoising. The performance of the NLM algorithm and wavelet thresholding approaches varies from pixel to pixel lying in different regions of an image. This paper presents a simple approach to estimate the original image pixel values by taking the weighted average of the denoised pixel values obtained by the NLM algorithm and some popular shrinking methods to reduce the artifacts. It assigns the weights to the denoised pixel values based on the region characteristics. The rest of the paper is organized as follows: a) The NLM algorithm is explained briefly in Section 2. b) Popular wavelet thresholding schemes such as BayesShrink and NeighShrink are discussed in Section 3. c) The proposed algorithm is presented in detail in Section 4. d) The experimental results and the choice of parameter settings are highlighted in Section 5. e) Finally, our conclusion is presented in Section 6.

2. Nonlocal means algorithm (NLM)

Let u_i and v_i be pixel values at location i in clean and noisy images U and V, respectively. The noisy image contains $i.i.d$ Gaussian noise η with distribution $\mathcal{N}(0, \sigma^2)$ and it can be modeled as:

$$v_i = u_i + \eta_i. \tag{1}$$

In the NLM algorithm [14], the estimated clean image pixel value $\hat{u}_i$ is obtained by taking the weighted average of all noisy pixels in a predefined search region S_i of size $S \times S$ as follows:

$$\hat{u}_i = \sum_{j \epsilon S_i} w'_{i,j}\, v_j, \tag{2}$$

where the parameters $w'_{i,j}$ are obtained as:

$$w'_{i,j} = \frac{e^{-\frac{\|v(N_i)-v(N_j)\|_2^2}{2P^2h^2}}}{\sum_{j \epsilon S_i} e^{-\frac{\|v(N_i)-v(N_j)\|_2^2}{2P^2h^2}}}. \tag{3}$$

The coefficients $w'_{i,j}$ represent the similarity between the local patches $v(N_i)$ and $v(N_j)$ of size $P \times P$ centered at pixels i and j in the search region S_i of size $S \times S$, respectively, which is computed by using the squared euclidean distance or norm $\|.\|_2^2$. The weights calculated in the search region using Eq. 3 ensure that $\sum_{j \epsilon S_i} w'_{i,j} = 1$. The smoothing parameter is generally chosen as $h = k'\sigma$, which depends on the standard deviation σ of Gaussian noise and some scaling constant k'. Parameter values such as $S = 21$, $P = 7$, and $k' = 0.75$ are taken in the NLM algorithm [14] to denoise the images. The main assumption of the NLM algorithm is patch regularity, which can be typically found in natural images but not in highly textured images. The NLM algorithm performs well for low noise levels, but it produces blurring and noise halo effects near image details at large noise levels.

3. Wavelet thresholding schemes

By performing the discrete wavelet transform (DWT) on noisy image V, the noisy wavelet coefficients $v^{(i)}$ can be modeled as:

$$v^{(i)} = u^{(i)} + \eta^{(i)}, \tag{4}$$

where $v^{(i)}$ and $u^{(i)}$ denote i^{th} noisy and noise-free wavelet coefficients, respectively. DWT is a multiresolution tool which decomposes the image into various frequency subbands denoted as LL_K, $LH_{k'}$, $HL_{k'}$, and $HH_{k'}$, where $k' = 1, 2, 3 \ldots . K$ represents the resolution level and K indicates the coarsest level. The subband LL_K represents the low frequency or approximation subband at resolution scale K, while $LH_{k'}$, $HL_{k'}$, and $HH_{k'}$ represent the horizontal, vertical, and diagonal details subbands of the image at resolution scale k', respectively. The subband HH_1 denotes the high frequency subband obtained using the first decomposition level, which is the most noisy subband among all subbands.

In the wavelet domain, the small- and large-magnitude wavelet coefficients correspond to noise and key signal details, respectively. To recover the signal with important details and less noise, the noisy wavelet coefficients are generally modified using an appropriate threshold. Choosing a small threshold value results in noisy signal, whereas a large threshold value leads to oversmoothing of the signal. Therefore, the selection of the appropriate threshold for wavelet shrinkage process is a very challenging task in wavelet-based image denoising algorithms. The selected threshold must be data-driven to take into account the information about region structures. The most popular data-driven thresholding schemes such as BayesShrink and NeighShrink are described as follows:

3.1. BayesShrink

Chang et al. [27] proposed the BayesShrink algorithm, which estimates the adaptive data-driven threshold derived in the Bayesian framework to modify noisy wavelet coefficients using soft thresholding. The estimated threshold obtained by the BayesShrink method is defined as follows:

$$T_B^{(i)} = \frac{\hat{\sigma}^2}{\hat{\sigma}_u^{(i)}}, \tag{5}$$

where $\hat{\sigma}^2$ and $\hat{\sigma}_u^{(i)}$ represent the estimated noise variance and signal standard deviation, respectively. The signal variance is estimated by taking the neighboring coefficients in a local window r_i of size $w \times w$ centered on noisy wavelet coefficient i. The original signal wavelet coefficients are estimated by applying adaptive threshold defined according to soft thresholding rule [27] as follows:

$$\hat{u}^{(i)} = sgn\left(v^{(i)}\right) . max\left(\left(|v^{(i)}| - T_B^{(i)}\right), 0\right), \tag{6}$$

where $\hat{u}^{(i)}$ denotes the estimated noise-free wavelet coefficient and $sgn(x)$ returns the sign of the parameter x.

3.2. NeighShrink

The NeighShrink image denoising algorithm proposed by Chen et al. [26] provides neighborhood-dependent threshold by exploiting the local correlation between the wavelet coefficients in a subband. Suppose S_i^2 is the sum of the squared noisy coefficients in a local window (r_i) of size $w \times w$ centered on each noisy wavelet coefficient i for a particular subband, which is defined as:

$$S_i^2 = \sum_{j \epsilon r_i} (v^{(j)})^2. \tag{7}$$

The shrinkage of noisy wavelet coefficients using the threshold $T_N^{(i)}$ can be expressed as:

$$\hat{u}^{(i)} = T_N^{(i)} v^{(i)}, \tag{8}$$

where $\hat{u}^{(i)}$ is the estimated noise-free wavelet coefficient, and the NeighShrink threshold $T_N^{(i)}$ is given as:

$$T_N^{(i)} = \left(1 - \frac{\lambda^2}{S_i^2}\right)_+, \tag{9}$$

where λ is the universal threshold whose value is given by $\lambda = \sigma\sqrt{2\ln(M)}$ and $(a)_+$ is equal to $\max(0, a)$. The main drawback of this algorithm is that the parameters such as fixed threshold λ and local window size are not data-driven, which provides a biased estimate of the mean square error (MSE). Dengwen et al. [28] proposed the Neigh-SUREShrink method that improves the performance of the NeighShrink algorithm by selecting the optimal threshold and local window size based on Stein's unbiased risk estimator (SURE) principle. This principle estimates the MSE between the estimated and original wavelet coefficients.

(a) (b) (c) (d)

Figure 1. Denoised Barbara image using various denoising methods at $\sigma = 30$: a) clean, b) NLM, c) BayesShrink, and d) NeighShrink.

4. Proposed approach

4.1. Motivation

In order to highlight the limitations of the NLM- and wavelet-based methods, the denoised results obtained by using the NLM [14], BayesShrink [27], and NeighShrink [26] algorithms at $\sigma = 30$ for the standard Barbara image are presented in Figure 1. It was observed that the NLM algorithm performs well for smooth regions mostly, but it produces more blurring effects near the image details. Wavelet-based schemes like BayesShrink and NeighShrink produces many artifacts in smooth regions of an image due to overthresholding of coefficients. However, they may preserve image details due to control on thresholding the noisy wavelet coefficients. Therefore, the performance of NLM algorithm and wavelet thresholding approaches may vary from pixel to pixel lying in different regions of an image. The core idea of the proposed algorithm is to take the weighted average of the denoised pixel values obtained by NLM and wavelet thresholding schemes, where the weights are adaptively selected on the basis of natural characteristics of local regions. This ensures that the filtering capabilities of both methods are effectively combined to further improve the denoising performance.

4.2. Fusion of NLM- and wavelet-based approaches

Suppose that D_{N_i} and D_{W_i} are the denoised pixel values obtained by applying the NLM algorithm [14] and wavelet thresholding approach BayesShrink [27]/NeighShrink [26] on noisy image, respectively. The final estimated image pixel value can be obtained by using the following expression:

$$D_i = w_i D_{N_i} + (1 - w_i) D_{W_i}, \tag{10}$$

where $w_i \epsilon [0, 1]$ is the weight assigned to i^{th} denoised pixel value, which is estimated by the NLM algorithm. A natural image usually contains both homogeneous (e.g., smooth) and heterogeneous (e.g., textures) regions, which can be characterized by using local features. Figure 2 illustrates various smooth and texture regions, respectively. In Figure 2a, region-1 and region-2 are purely smooth regions, whereas Figure 2b represents two different types of regions with high texture: 1) an artificial generated region-1, and 2) a natural texture region-2 obtained from the Baboon image. Now, to get the basic estimate of these regions, the NLM [14] and BayesShrink [27] algorithms are applied on noisy image for $\sigma = 30$. The denoised image pixel values obtained using the NLM and BayesShrink methods are weighted by weights w and $1 - w$, respectively, to obtain the final denoised image D. The variation of MSE with respect to weight w is also analyzed for various regions at $\sigma = 30$ in Figures 2c and 2d. For smooth regions, it was observed that the MSE between the original and

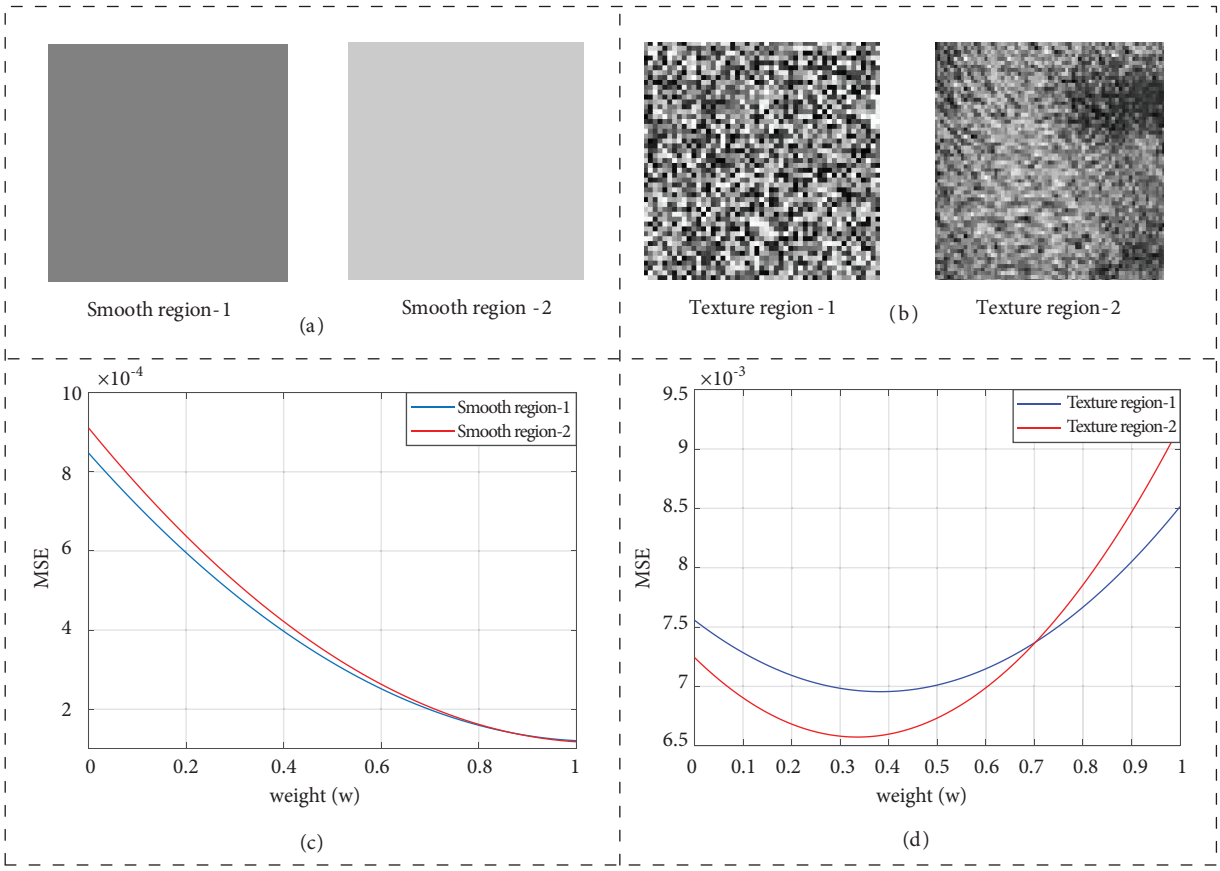

Figure 2. Variation in MSE with respect to weight w for various regions using Eq. (10).

estimated regions decreases as the value of weight w increases. It means that the estimated pixel value by the NLM algorithm must be given higher weight in comparison with the BayesShrink method to minimize the MSE for smooth regions. Similarly, the MSE decreases first and then increases as the value of weight w increases for texture regions. Moreover, the weight w required to ensure minimum MSE in this case is less as compared to that in Figure 2c. This implies that the wavelet-based algorithm must be given higher weight $(1-w)$ in comparison with the NLM. Thus, the combination of the NLM and BayesShrink can reduce MSE for a suitable value of w, which should be selected according to region characteristics.

4.3. Determination of region characteristics

To assign weight w to the denoised pixel as defined in Eq. (10), the characterization of image regions is required, which can be accomplished by some local features that can effectively distinguish regions having different characteristics in an image. For example, the local variance can be employed to capture the change in gray levels in a local neighborhood.

$$\sigma^2_{\Omega_i} = \frac{1}{n \times n} \sum_{j \epsilon \Omega_i} (v_j - \overline{v}_i)^2 . \tag{11}$$

The small and large values of local variance indicate smooth and texture regions, respectively. Assume that a local neighborhood Ω_i of size $n \times n$ is centered on pixel i in the noisy image. The change in the gray levels

in the local window Ω_i is expressed above, where $\overline{v}_i$ denotes the local mean for pixel i. Figure 3 shows the

(a) (b) (c)

Figure 3. Variance map of Barbara image: a) clean, b) $\sigma = 20$, and c) $\sigma = 30$.

variance map of clean and noisy Barbara image for different noise levels $\sigma = 20$ and 30. It can be observed that the black and white regions correspond to smooth and texture regions in the map, respectively. The change in the gray levels of the variance map reflects the change in local characteristics of various regions of the image. The weight w_i is obtained by normalizing the variance map of an image. Let σ^2_{max} and σ^2_{min} be minimum and maximum local variances in a variance map of image. To obtain w_i, the normalization of the variance map can be done as:

$$w_i = \frac{\sigma^2_{max} - \sigma^2_{\Omega_i}}{\sigma^2_{max} - \sigma^2_{min}}. \tag{12}$$

It means that the denoised pixel lying in the region having a small variance gets more weights. Similarly, a pixel lying in the regions having a large variance is less weighted in Eq. 11. Figure 4 shows the block diagram of the proposed algorithm.

5. Experimental results

The performance of the proposed approach is measured qualitatively and quantitatively in terms of peak signal-to-noise ratio (PSNR(dB)), mean structural similarity index measure (MSSIM) [39], and visual quality, respectively, by performing extensive simulation on various natural[1] and texture[2] images of size 256×256 for different noise levels $\sigma = 20$, 30, 40, and 50 as shown in Figures 5 and 6. Various spatial and transform domain state-of-the-art methods like the entropy-based bilateral filter (EBF) [7], NLM algorithm [14] and its recent variant [17], wavelet shrinkage methods such as BayesShrink [27], NeighShrink [26], and NeighSUREShrink [28] are considered in the proposed approach. The parameter settings of these state-of-the-art methods are taken as suggested by their corresponding authors. For the NLM algorithm [14], the size of the search region and patch are taken as 21×21 and 7×7, respectively. The value of scaling constant k' in the smoothing parameter ($h = k'\sigma$) is chosen as 0.75. The number of the decomposition levels is four and the wavelet family for all wavelet-based approaches is symlet (sym8). The size of local neighborhood is chosen as $n = 7$ to

[1] *Available link: https://www.cs.cmu.edu/~cil/v-images.html*
[2] *Available link: http://www.ux.uis.no/ tranden/brodatz.html*

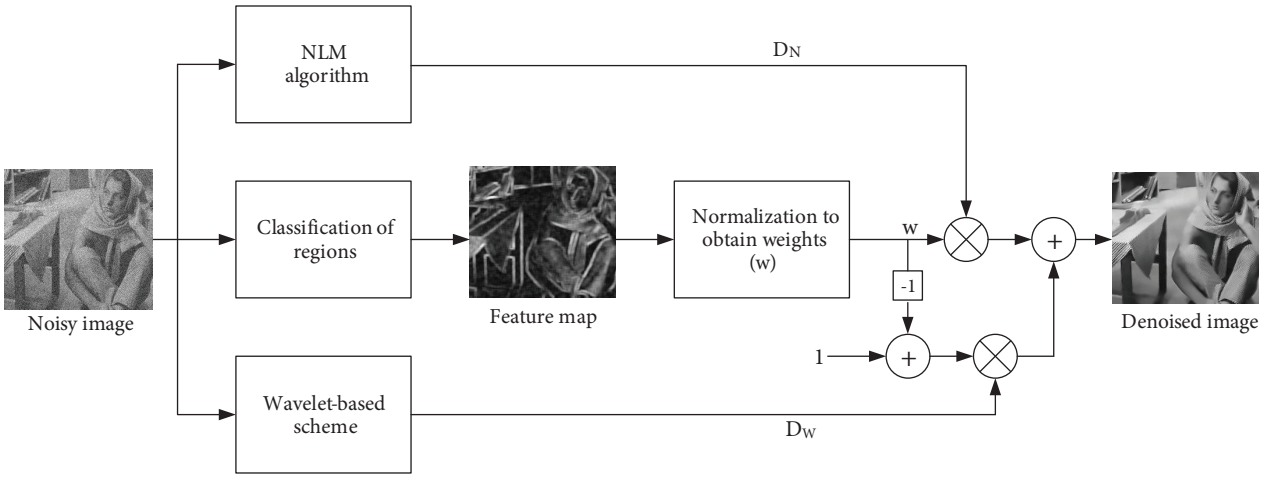

Figure 4. Block diagram of the proposed algorithm

.

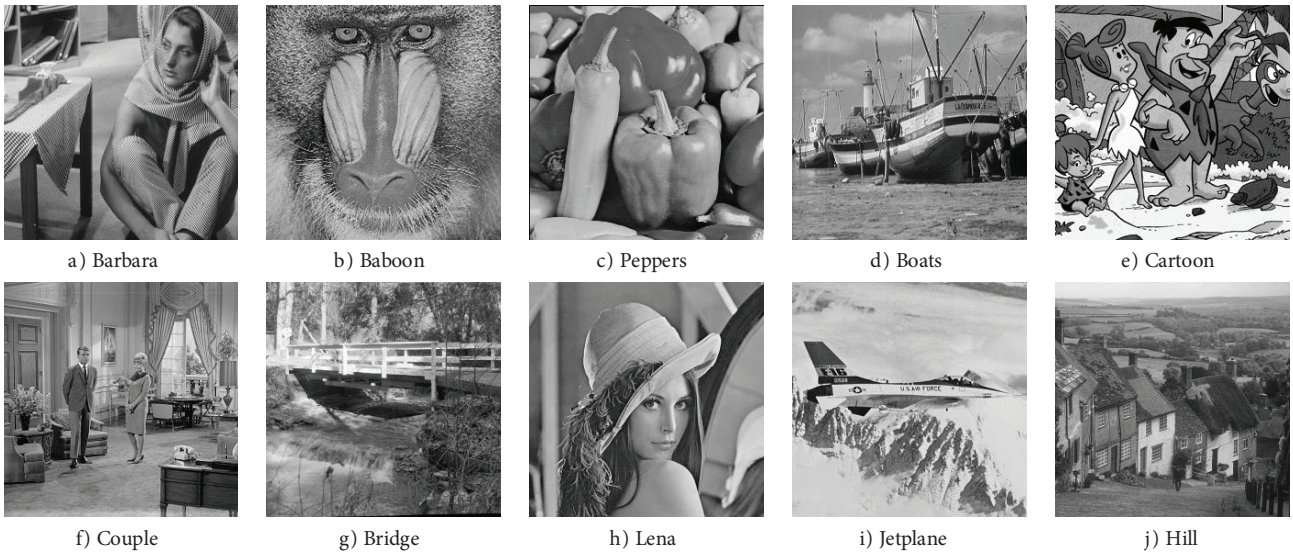

Figure 5. Various standard natural images used in all experiments

obtain the variance map of an image. The NLM algorithm is combined with the BayesShrink, NeighShrink, and NeighSURE methods to improve their performance. Recent methods like the EBF and ANLM are also combined with the NeighSUREShrink algorithm to enhance the performance. Tables 1 and 2 show the denoising results of various combinations of benchmark techniques in terms of PSNR(dB) and MSSIM for various images at different noise levels, respectively. It was observed that the performance of the NLM algorithm deteriorates at high noise levels, especially for standard texture images such as Baboon, Cartoon, and Bridge, whereas the wavelet-based approaches like NeighShrink and NeighSUREShrink perform better than NLM for these images at high noise levels. As the performance of these methods varies from region to region in an image, it is improved by exploiting the corresponding weighted denoised pixel values. The weight is changed dynamically on the basis of region characteristics. The NLM+BayesShrink algorithm achieves better performance than the NLM- and wavelet-based shrinkage methods with a PSNR gain of 0.2–1.0 dB for almost all images at various noise levels. The combination of NLM with NeighSUREShrink yields promising denoising results at high noise level

$\sigma > 30$. Similarly, the combination of EBF and ANLM with the wavelet shrinkage methods provides significant improvement in their performance. To judge the visual quality of the denoised images, three sample images with different characteristics viz. Lena, Baboon, and Peppers selected from Figure 5 are shown in Figures 7–9 for $\sigma = 30$. It was observed that the artifacts produced by the NLM and other wavelet methods can be reduced by combining these approaches on the basis of region characteristics. It can be concluded that the combination of NLM, EBF, and ANLM with the wavelet methods preserves the important image details effectively.

In order to judge the efficacy of the proposed method for texture images, its performance is also compared with a patch-based denoising method. The performance of the proposed approach and BM3D algorithm [36] is tested for Baboon and randomly chosen texture images from Brodatz texture album as shown in Figure 6. BM3D method is the most effective and current state-of-the-art image denoising algorithm, which provides

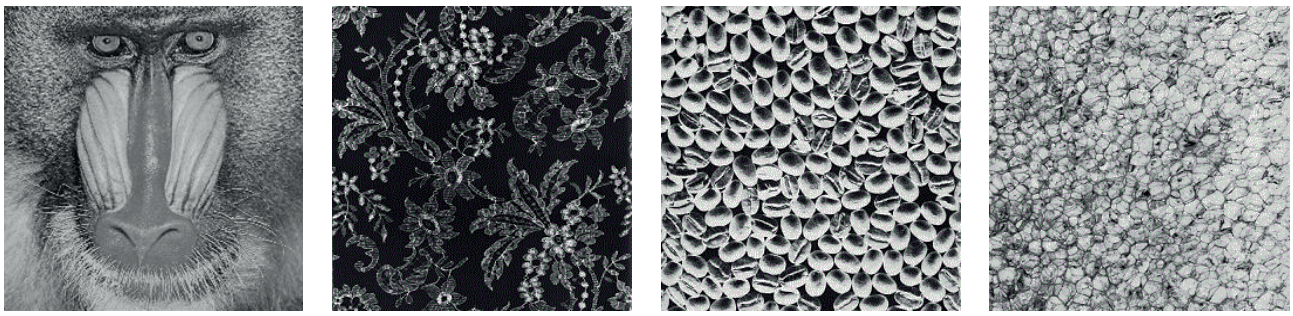

(a) (b) (c) (d)

Figure 6. Various texture images: a) Baboon and b) Brodatz album (D40, D74, and D112)

promising denoising results for images having large redundancy. As most of the patch-based methods are based on BM3D framework, the performance of the proposed approach is here compared with the BM3D algorithm. Table 3 shows the denoising results of the proposed approach (ANLM+NeighSURE) and BM3D for natural and texture images at different noise levels in terms of PSNR(dB). As shown in Table 3, the proposed approach obtains a PSNR gain of 0.2–0.5 dB for $\sigma \geq 30$ over BM3D method. Figure 10 depicts the visual quality of the denoised images by the proposed approach and BM3D method. It was clearly observed that the proposed approach is suitable for filtering texture images and is also computationally less expensive compared to BM3D.

Table 4 shows the comparison of the computational complexities involved in the implementation of the NLM, wavelet-based, BM3D methods, and the proposed method, where M, S, and P indicate the total number of pixels in an image, search region size, and patch size, respectively. N_2 denotes the total number of similar patches in a group in the BM3D algorithm. $O_{T_{2D}}$ and $O_{T_{3D}}$ are the arithmetic operations required to perform 2D and 3D transform on group of similar patches, respectively [36]. Generally, the patch and search region sizes used for BM3D are larger than those in NLM. For example, $P = 7$, $S = 21$ for NLM and $P = 8$, $S = 39$ for BM3D imply the higher computational complexity. Moreover, BM3D is iterative in nature, which further increases its complexity involved in its implementation.

6. Conclusion

This paper presents a simple and novel approach which preserves the key image details by fusion of the denoised pixel values obtained through spatial and transform domain techniques based on region characteristics. Experimental results show that the denoising performance of EBF, NLM, its variants, and wavelet-based approaches can be further improved by applying the proposed approach. The PSNR gain achieved by combination

Table 1. Denoising results (PSNR(dB)) of the proposed algorithm and other benchmark techniques for various images at different noise levels.

Methods	σ	Barbara	Baboon	Peppers	Boats	Cartoon	Couple	Bridge	Lena	Jetplane	Hill
NLM [14]	20	27.2439	24.5938	29.3576	26.5448	24.5743	26.3391	25.5228	28.6974	27.7715	26.8383
	30	24.9526	21.9845	27.2262	24.4503	22.1873	23.9063	23.4884	26.3736	25.7334	24.6260
	40	23.0126	20.7786	25.3432	22.8733	20.3857	22.4268	22.2542	24.7014	23.8238	23.5105
	50	21.7849	20.1770	23.9479	21.8564	18.7532	21.6211	21.4224	23.3432	22.6452	22.6364
Bayes-Shrink [27]	20	26.3027	23.9405	28.4353	26.4888	24.4139	26.3124	25.6710	27.7755	27.2894	26.6361
	30	24.0951	22.0428	26.0026	24.2347	21.8509	23.9688	23.5516	25.4311	24.8188	24.4502
	40	22.6004	20.8324	24.0241	22.6301	20.0196	22.4464	22.2423	23.4353	23.0565	23.0224
	50	21.4184	19.9482	22.4872	21.4690	18.6744	21.2653	21.0021	22.1626	21.7772	21.8852
Neigh-Shrink [26]	20	26.6063	24.1324	29.0161	26.9380	24.4462	26.6387	25.8515	28.3103	27.6387	27.0586
	30	24.5247	22.3752	26.5195	24.8069	21.9915	24.2644	24.0337	25.9497	25.4568	25.1262
	40	23.1195	21.2157	24.7938	23.3077	20.2418	23.0698	22.7670	24.4371	23.9192	23.7659
	50	22.1862	20.4819	23.7053	22.2224	19.0219	21.9695	21.8131	23.2262	22.7148	23.7309
Neigh-SURE [28]	20	26.8736	25.0630	29.0918	26.9890	24.7591	26.7789	26.1803	28.3316	27.7531	27.1566
	30	24.8201	22.9705	26.7006	24.8696	22.0566	24.5389	24.2146	26.1621	25.5990	25.3200
	40	23.3757	21.6576	25.2844	23.5868	20.3344	23.0333	23.0695	24.8565	24.2928	24.1484
	50	22.3771	20.6505	24.0400	22.6460	19.0432	22.4329	22.1723	23.9590	23.3374	23.3400
EBF [7]	20	26.0645	23.7197	30.1631	27.1219	25.1682	26.4524	26.0230	28.9914	28.6759	27.4069
	30	24.1690	22.0060	27.7618	25.2301	22.5956	24.6988	24.5716	26.8529	26.3852	25.7501
	40	22.8799	21.3972	25.8573	23.7020	20.9926	23.3813	23.3494	25.3329	24.7210	24.6005
	50	22.0223	20.7750	24.2769	22.8222	19.6744	22.3711	22.6090	24.1810	23.5327	23.6025
ANLM [17]	20	28.0449	24.9454	30.3218	27.6758	26.5315	27.2806	26.5018	29.3185	28.7853	27.7593
	30	25.3881	22.8371	27.8523	25.6903	23.8045	24.8399	24.4957	27.1589	26.6434	25.6720
	40	23.8092	21.6338	26.0200	23.8823	21.7591	23.3684	23.1281	25.5799	24.8859	24.3764
	50	22.6072	20.8913	24.4808	22.8429	20.0833	22.3992	22.2841	24.3370	23.6256	23.3958
NLM + Bayes-Shrink	20	27.6323	24.8066	29.7476	27.0484	25.2815	26.8573	25.9617	29.0153	28.2594	27.3106
	30	25.3102	22.4456	27.6144	25.0500	22.7765	24.5829	24.0616	26.7797	26.1221	25.2605
	40	23.5237	21.3505	25.7919	23.5911	20.8564	23.1750	22.9491	25.2615	24.3838	24.2165
	50	22.3867	20.6471	24.4826	22.5892	19.4061	22.3975	22.0587	23.8902	23.2964	23.2436
NLM + Neigh-Shrink	20	27.5536	24.5589	29.8038	26.9709	25.3367	26.7017	26.059	28.9656	28.2210	27.3215
	30	24.9536	22.3812	27.3929	24.9363	22.6694	24.4901	24.2668	26.5067	25.8509	25.3175
	40	23.4130	21.4820	25.6268	23.5286	20.5856	23.1648	22.9886	24.9148	24.1793	24.1237
	50	22.3407	20.6664	24.4010	22.5254	19.2460	22.3112	22.1093	23.7532	22.9555	23.2531
NLM + Neigh-SURE	20	27.4659	25.1602	29.7464	27.3120	24.9707	27.0779	26.4179	28.8638	28.1103	27.4535
	30	25.4071	23.0267	27.4770	25.1305	22.4470	24.7556	24.4807	26.7220	26.0973	25.6135
	40	23.7602	21.7512	25.9220	23.6971	20.8199	23.3854	23.2716	25.2877	24.5094	24.3956
	50	22.5790	20.8786	24.6369	22.7698	19.3919	22.4971	22.3414	24.2721	23.4290	23.6513
EBF + Neigh-SURE	20	26.8116	24.7388	30.3447	27.5388	25.6938	26.9671	26.3935	29.1830	28.7531	27.7083
	30	24.8972	23.0062	27.9297	25.4953	23.0384	25.0506	24.8674	27.0655	26.6173	26.0406
	40	23.5667	21.8170	26.1607	24.1576	21.1677	23.7723	23.6686	25.5176	24.9251	24.8338
	50	22.6316	21.0689	24.9269	23.0909	19.8472	22.8358	22.8162	24.4909	23.8574	24.0022
ANLM + Neigh-SURE	20	28.1952	25.2399	30.4014	27.7964	26.6283	27.4528	26.6506	29.4072	28.7745	27.8875
	30	25.3541	23.1236	27.9667	25.8124	23.7637	25.0811	24.7064	27.3029	26.7288	25.9505
	40	24.0482	21.9527	26.2681	24.1286	21.6602	23.7396	23.4713	25.8332	25.0822	24.7288
	50	22.9527	21.1504	24.8575	23.2016	20.2274	22.7795	22.7032	24.7235	23.8404	23.9154

Table 2. Denoising results (MSSIM) of the proposed algorithm and other benchmark techniques for various images at different noise levels.

Methods	σ	Barbara	Baboon	Peppers	Boats	Cartoon	Couple	Bridge	Lena	Jetplane	Hill
NLM [14]	20	0.8389	0.7242	0.8515	0.7467	0.8669	0.7410	0.6974	0.8298	0.8350	0.7045
	30	0.7432	0.5403	0.7985	0.6566	0.7924	0.6192	0.5688	0.7612	0.7721	0.5953
	40	0.6506	0.4325	0.7247	0.5799	0.7142	0.5349	0.4929	0.7009	0.7083	0.5356
	50	0.5907	0.3777	0.6865	0.5297	0.6192	0.4848	0.4446	0.6453	0.6479	0.4907
Bayes-Shrink [27]	20	0.7865	0.6995	0.7703	0.7400	0.8326	0.7384	0.7338	0.7627	0.7611	0.6980
	30	0.6864	0.5910	0.6806	0.6295	0.7547	0.6261	0.6263	0.6510	0.6539	0.5881
	40	0.6044	0.5062	0.5776	0.5388	0.6812	0.5293	0.5412	0.5614	0.5716	0.5062
	50	0.5381	0.4281	0.5137	0.4712	0.6114	0.4587	0.4689	0.4913	0.5007	0.4437
Neigh-Shrink [26]	20	0.7977	0.6939	0.8051	0.7568	0.8348	0.7573	0.7405	0.7888	0.7958	0.7199
	30	0.7083	0.5893	0.7125	0.6574	0.7608	0.6576	0.6400	0.6978	0.6933	0.6207
	40	0.6333	0.4996	0.6470	0.5717	0.6916	0.5704	0.5645	0.6133	0.6203	0.5377
	50	0.5683	0.4295	0.5734	0.5209	0.6247	0.5005	0.5029	0.5454	0.5501	0.4882
Neigh-SURE [28]	20	0.8048	0.7720	0.8163	0.8347	0.7627	0.7631	0.7702	0.7953	0.8106	0.7336
	30	0.7196	0.6589	0.7593	0.7557	0.6682	0.6718	0.6637	0.7272	0.7498	0.6334
	40	0.6498	0.5514	0.7034	0.6872	0.6062	0.6016	0.5928	0.6794	0.6946	0.5745
	50	0.6029	0.4746	0.6622	0.6319	0.5489	0.5428	0.5370	0.6306	0.6517	0.5225
EBF [7]	20	0.7860	0.6661	0.8142	0.7634	0.8359	0.7441	0.7236	0.7922	0.8002	0.7345
	30	0.7105	0.5815	0.7465	0.6768	0.7584	0.6627	0.6558	0.7147	0.7364	0.6350
	40	0.6401	0.5711	0.7015	0.6172	0.6906	0.5979	0.5888	0.6700	0.6847	0.5768
	50	0.5785	0.4672	0.6531	0.5709	0.6347	0.5401	0.5327	0.6297	0.6270	0.5251
ANLM [17]	20	0.8433	0.7510	0.8479	0.7826	0.8946	0.7735	0.7553	0.8303	0.8403	0.7482
	30	0.7509	0.6220	0.7821	0.6948	0.8276	0.6682	0.6505	0.7589	0.7747	0.6499
	40	0.6725	0.5259	0.7217	0.6168	0.7596	0.5880	0.5742	0.6924	0.7200	0.5725
	50	0.5950	0.4529	0.6646	0.5663	0.6876	0.5240	0.5074	0.6290	0.6577	0.5170
NLM + Bayes-Shrink	20	0.8424	0.7308	0.8567	0.7664	0.8771	0.7601	0.7221	0.8365	0.8408	0.7274
	30	0.7529	0.5873	0.8027	0.6851	0.8067	0.6577	0.6143	0.7681	0.7734	0.6310
	40	0.6697	0.5087	0.7388	0.6104	0.7353	0.5803	0.5456	0.7006	0.7101	0.5651
	50	0.6084	0.4343	0.6923	0.5529	0.6571	0.5220	0.4955	0.6314	0.6540	0.5121
NLM + Neigh-Shrink	20	0.8442	0.7260	0.8591	0.7659	0.8757	0.7653	0.7450	0.8388	0.8428	0.7274
	30	0.7515	0.5917	0.8036	0.6706	0.8043	0.6639	0.6406	0.7757	0.7770	0.6287
	40	0.6566	0.5120	0.7494	0.5867	0.7325	0.5783	0.5655	0.7068	0.7174	0.5526
	50	0.5914	0.4432	0.6992	0.5378	0.6349	0.5119	0.5069	0.6471	0.6549	0.5066
NLM + Neigh-SURE	20	0.8183	0.7736	0.8290	0.8444	0.7701	0.7709	0.7711	0.8076	0.8219	0.7405
	30	0.7384	0.6648	0.7791	0.7714	0.6728	0.6760	0.6648	0.7452	0.7653	0.6382
	40	0.6669	0.5669	0.7270	0.6896	0.6075	0.6038	0.5967	0.7015	0.7135	0.5793
	50	0.6179	0.4898	0.6932	0.5725	0.5499	0.5445	0.5402	0.6551	0.6675	0.5304
EBF + Neigh-SURE	20	0.7959	0.7754	0.8337	0.7665	0.8666	0.7658	0.7699	0.8079	0.8424	0.7448
	30	0.7265	0.6640	0.7822	0.6928	0.7973	0.6701	0.6605	0.7480	0.7743	0.6422
	40	0.6563	0.5653	0.7316	0.6201	0.7337	0.6065	0.6097	0.6772	0.6960	0.5845
	50	0.6001	0.4882	0.6995	0.5793	0.6789	0.5421	0.5653	0.6318	0.6417	0.5823
ANLM + Neigh-SURE	20	0.8468	0.7714	0.8539	0.7920	0.8985	0.7836	0.7690	0.8363	0.8429	0.7572
	30	0.7619	0.6522	0.7955	0.7082	0.8329	0.6870	0.6678	0.7705	0.7808	0.6613
	40	0.6914	0.5612	0.7463	0.6371	0.7611	0.6168	0.5965	0.7140	0.7318	0.5983
	50	0.6227	0.4865	0.7020	0.5907	0.6923	0.5551	0.5416	0.6590	0.6771	0.5521

Figure 7. Denoised Lena image using various methods for $\sigma = 30$: a) clean, b) NLM, c) BayesShrink, d) NeighShrink, e) NeighSUREShrink, f) EBF, g) ANLM, h) NLM+BayesShrink, i) NLM+NeighShrink, j) NLM+NeighSUREShrink, k) EBF+ NeighSUREShrink, and l) ANLM+NeighSUREShrink.

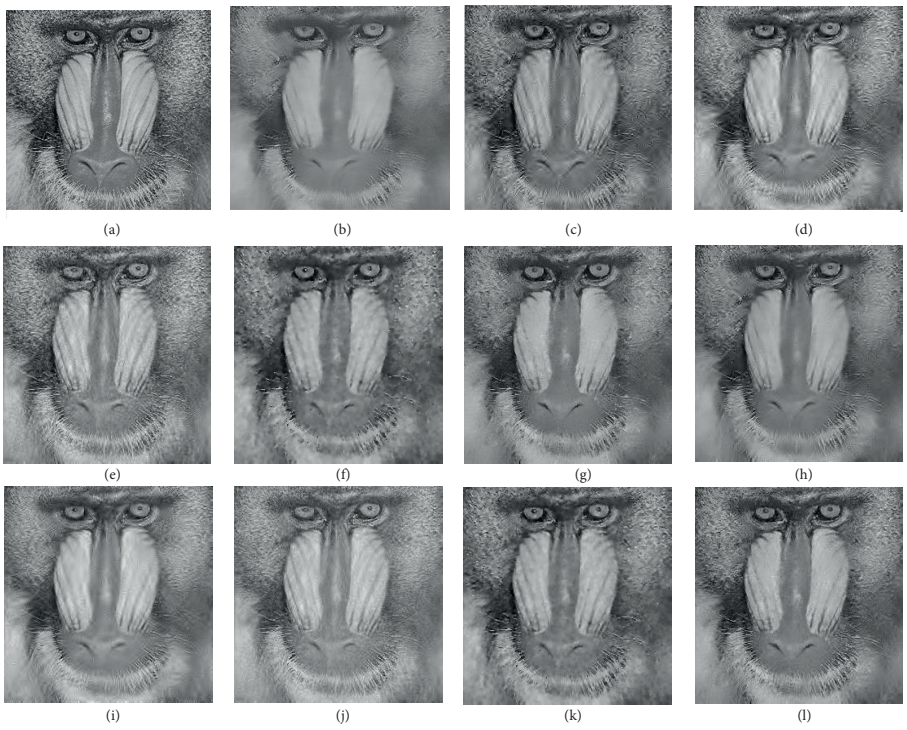

Figure 8. Denoised Baboon image using various methods for $\sigma = 30$: a) clean, b) NLM, c) BayesShrink, d) NeighShrink, e) NeighSUREShrink, f) EBF, g) ANLM, h) NLM+BayesShrink, i) NLM+NeighShrink, j) NLM+NeighSUREShrink, k) EBF+ NeighSUREShrink, and l) ANLM+NeighSUREShrink.

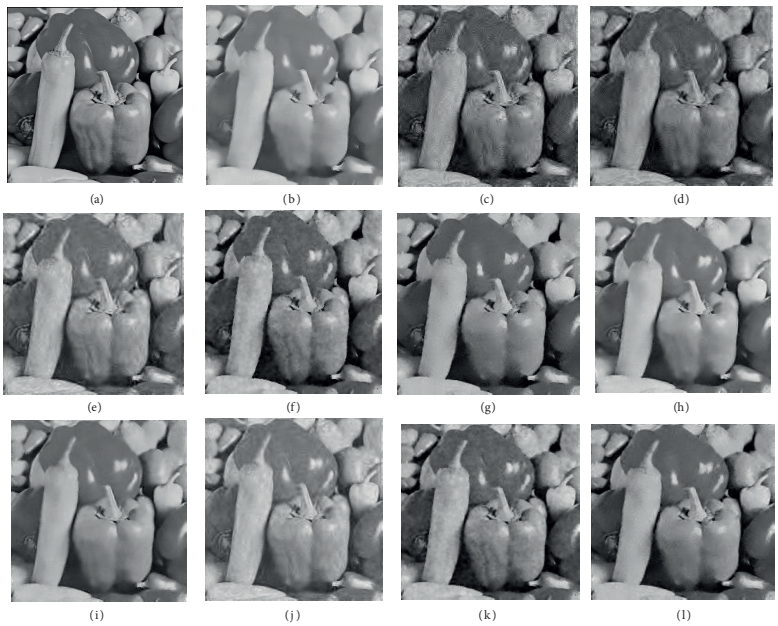

Figure 9. Denoised Peppers image using various methods for $\sigma = 30$: a) clean, b) NLM, c) BayesShrink, d) NeighShrink, e) NeighSUREShrink, f) EBF, g) ANLM, h) NLM+BayesShrink, i) NLM+NeighShrink, j) NLM+NeighSUREShrink, k) EBF+ NeighSUREShrink, and l) ANLM+NeighSUREShrink.

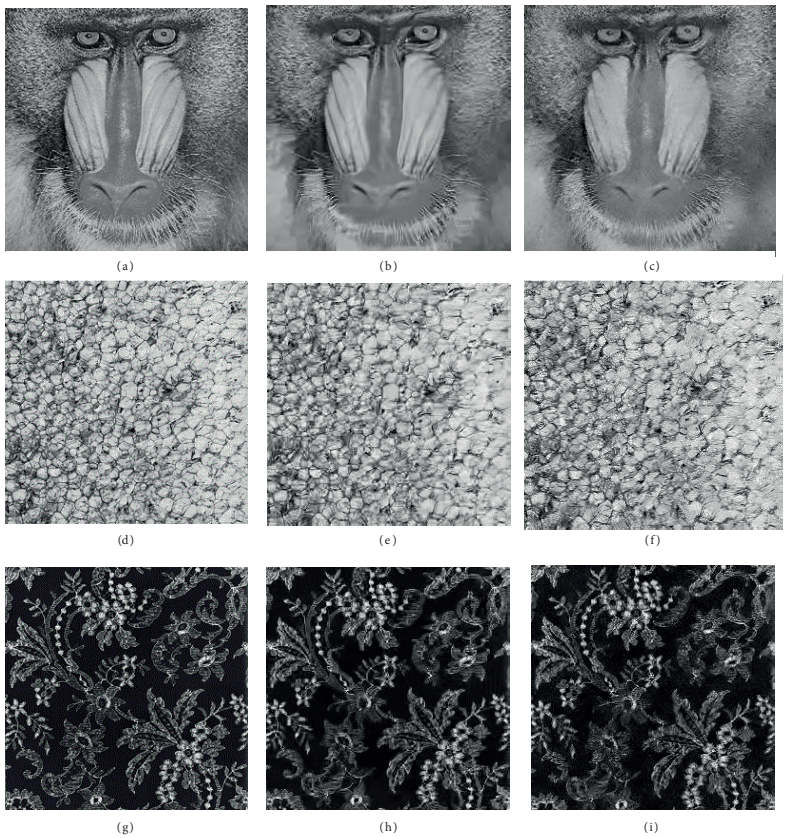

Figure 10. Denoised texture image (Baboon, D40, and D112) using various methods for $\sigma = 30$: a) First column corresponds to clean images, b) Second column corresponds to denoised images using BM3D method, c) Third column corresponds to denoised images using the proposed approach (ANLM+NeighShrink).

Table 3. Denoising results (PSNR(dB)) of the proposed approach and BM3D technique for various texture images at different noise levels.

Methods	σ	Baboon	D40	D74	D112
BM3D [36]	20	25.3215	23.7145	26.6917	23.3622
	30	23.0561	20.9981	20.9504	20.6876
	40	21.6258	19.2674	19.2448	19.0220
	50	20.8571	18.0374	18.0938	17.9371
ANLM + Neigh-SURE	20	25.2440	23.7725	23.7073	23.5221
	30	23.1900	21.2881	21.3859	20.9806
	40	22.0181	19.7354	19.5065	19.4041
	50	21.1547	18.5636	18.3154	18.3091

Table 4. Computational complexity of various methods.

Methods	NLM [14]	Wavelet-based [26–28]	BM3D [36]	Proposed
Computational complexity	$\mathcal{O}(MS^2P^2)$	$\mathcal{O}(M) - \mathcal{O}(M \log M)$	$\mathcal{O}(MO_{T_{2D}}(P^2))+\mathcal{O}(M\left(\frac{(P^2+N_2)S^2}{N_{step}^2}\right))$ $+\mathcal{O}(MO_{T_{3D}}\left(\frac{P^2N_2}{N_{step}^2}\right))$	$\mathcal{O}(MS^2P^2) + \mathcal{O}(M)$ $+(\mathcal{O}(M) - \mathcal{O}(M \log M))$

of various methods in the proposed approach lies in the range of 0.2–1 dB. The present scheme also results in better performance in comparison with the patch-based denoising scheme like BM3D for texture images at lower computational complexity. With the application of the proposed approach, the key image details are also well preserved at high noise levels.

References

[1] Bovik AC. The Essential Guide to Image Processing. Burlington, MA, USA: Academic Press, 2009.

[2] Gonzalez RC, Woods RE. Digital Image Processing. 2nd ed. Beijing, China: Publishing House of Electronics Industry, 2002.

[3] Chatterjee P, Milanfar P. Is denoising dead? IEEE T Image Process 2010; 19: 895-911.

[4] Milanfar P. A tour of modern image filtering: new insights and methods, both practical and theoretical. IEEE Signal Proc Mag 2013; 30: 106-28.

[5] Jain P, Tyagi V. Spatial and frequency domain filters for restoration of noisy images. IETE Journal of Education 2013; 54: 108-16.

[6] Tomasi C, Manduchi R. Bilateral filtering for gray and color images. In: Computer Vision, 1998. Sixth International Conference on 1998 Jan 4; Bombay, India. IEEE. pp. 839-846.

[7] Dai T, Lu W, Wang W, Wang J, Xia ST. Entropy-based bilateral filtering with a new range kernel. Signal Process 2017; 137: 223-34.

[8] Buades A, Coll B, Morel JM. A non-local algorithm for image denoising. In: Computer Vision and Pattern Recognition, 2005. CVPR 2005. IEEE Computer Society Conference 2005; San Diego, CA, USA. IEEE. pp. 60-65.

[9] Buades A, Coll B, Morel JM. A review of image denoising algorithms, with a new one. Multiscale Model Sim 2005; 4: 490-530.

[10] Rakheja P, Vig R. Image denoising using various wavelet transforms: a survey. Indian Journal of Science and Technology 2017; 9: 1-7.

[11] Xiao F, Zhang Y. A comparative study on thresholding methods in wavelet-based image denoising. Procedia Engineer 2011; 15: 3998-4003.

[12] De la Rosa Vargas JI, Villa JJ, González E, Cortez J. A tour of nonlocal means techniques for image filtering. In: Electronics, Communications and Computers (CONIELECOMP), 2016 International Conference. Cholula, Mexico. IEEE. pp. 32-39.

[13] Mahmoudi M, Sapiro G. Fast image and video denoising via nonlocal means of similar neighborhoods. IEEE Signal Proc Let 2005; 12: 839-42.

[14] Van De Ville D, Kocher M. SURE-Based Non-Local Means. IEEE Signal Proc Let 2009; 16: 973-976.

[15] Riot P, Almansa A, Gousseau Y, Tupin F. A correlation-based dissimilarity measure for noisy patches. In: International Conference on Scale Space and Variational Methods in Computer Vision.4–8 June 2017; Kolding, Denmark. Springer, Cham. pp. 184-195.

[16] Zhong H, Yang C, Zhang X. A new weight for nonlocal means denoising using method noise. IEEE Signal Proc Let 2012; 19: 535-538.

[17] Verma R, Pandey R. A statistical approach to adaptive search region selection for NLM-based image denoising algorithm. Multimed Tools Appl 2018; 77: 549-66.

[18] Wu Y, Tracey B, Natarajan P, Noonan JP. James–Stein type center pixel weights for non-local means image denoising. IEEE Signal Proc Let 2013; 20: 411-414.

[19] Wu Y, Tracey B, Natarajan P, Noonan JP. Probabilistic non-local Means IEEE Signal Proc Let 2013; 20: 763-766.

[20] Ghosh S, Mandal AK, Chaudhury KN. Pruned non-local means. IET Image Process 2017; 11: 317-323.

[21] Jain P, Tyagi V. A survey of edge-preserving image denoising methods. Inform Syst Front 2016; 18: 159-70.

[22] Kazubek M. Wavelet domain image denoising by thresholding and Wiener filtering. IEEE Signal Proc Let 2003; 10: 324-326.

[23] Donoho DL. De-noising by soft-thresholding. IEEE T Inform Theory 1995; 41: 613-627.

[24] Donoho DL, Johnstone IM. Adapting to unknown smoothness via wavelet shrinkage. J Am Stat Assoc 1995; 90: 1200-1224.

[25] Zhang XP, Desai MD. Adaptive denoising based on SURE risk. IEEE Signal Proc Let 1998; 5: 265-267.

[26] Chen GY, Bui TD, Krzyżak A. Image denoising with neighbour dependency and customized wavelet and threshold. Pattern Recogn 2005; 38: 115-124.

[27] Chang SG, Yu B, Vetterli M. Adaptive wavelet thresholding for image denoising and compression. IEEE T Image Process 2000; 9: 1532-1546.

[28] Dengwen Z, Wengang C. Image denoising with an optimal threshold and neighbouring window. Pattern Recogn Lett 2008; 29: 1694-1697.

[29] Mihcak MK, Kozintsev I, Ramchandran K, Moulin P. Low-complexity image denoising based on statistical modeling of wavelet coefficients. IEEE Signal Proc Let 1999; 6: 300-303.

[30] Sendur L, Selesnick IW. Bivariate shrinkage with local variance estimation. IEEE Signal Proc Let 2002; 9: 438-441.

[31] Om H, Biswas M. An improved image denoising method based on wavelet thresholding. Journal of Signal and Information Processing 2012; 3: 109-116.

[32] Jiang J, Guo J, Fan W, Chen Q. An improved adaptive wavelet denoising method based on neighboring coefficients. In: Intelligent Control and Automation (WCICA), 2010 8th World Congress on Jul 7 2010; China. IEEE. pp. 2894-2898.

[33] Om H, Biswas M. A generalized image denoising method using neighbouring wavelet coefficients. Signal Image Video P 2015; 9: 191-200.

[34] Jain P, Tyagi V. LAPB: locally adaptive patch-based wavelet domain edge-preserving image denoising. Inform Sciences 2015; 294: 164-181.

[35] Lebrun M, Buades A, Morel JM. A nonlocal bayesian image denoising algorithm. Siam J Imaging Sci 2013; 6: 1665-1688.

[36] Dabov K, Foi A, Katkovnik V, Egiazarian K. Image denoising by sparse 3-D transform-domain collaborative filtering. IEEE T Image Process 2007; 16: 2080-2095.

[37] Pierazzo N, Rais ME, Morel JM, Facciolo G. DA3D: fast and data adaptive dual domain denoising. InICIP 2015 Sep 27; IEEE pp. 432-436.

[38] Liu J, Liu R, Wang Y, Chen J, Yang Y, Ma D. Image denoising searching similar blocks along edge directions. Signal Process-Image 2017; 57: 33-45.

[39] Wang Z, Bovik AC, Sheikh HR, Simoncelli EP. Image quality assessment: from error visibility to structural similarity. IEEE T Image Process 2004; 13: 600-612.